journal

J. Am. Ceram. Soc., **81** [11] 2821–30 (1998)

Microstructural Design of Silicon Nitride with Improved Fracture Toughness: I, Effects of Grain Shape and Size

Paul F. Becher,* Ellen Y. Sun,* Kevin P. Plucknett,*,† Kathleen B. Alexander,*,# Chun-Hway Hsueh,* Hua-Tay Lin,* Shirley B. Waters, and C. Gary Westmoreland

Oak Ridge National Laboratory, Oak Ridge, Tennessee 37831-6068

Eul-Son Kang

Agency for Defense Development, Taejon, Republic of Korea

Kiyoshi Hirao* and Manuel E. Brito*

National Industrial Research Institute, Nagoya, Japan

The use of self-reinforcement by larger elongated grains in silicon nitride ceramics requires judicious control of the microstructure to achieve high steady-state toughness and high fracture strength. With a distinct bimodal distribution of grain diameters, such as that achieved by the addition of 2% rodlike seeds, the fracture resistance rapidly rises with crack extension to steady-state values of up to 10 MPa·m$^{1/2}$ and is accompanied by fracture strengths in excess of 1 GPa. When the generation of elongated reinforcing grains is not regulated, a broad grain diameter distribution is typically generated. While some toughening is achieved, both the plateau (steady-state) toughness and the *R*-curve response suffer, and the fracture strength undergoes a substantial reduction. Unreinforced equiaxed silicon nitride exhibits the least *R*-curve response with a steady-state toughness of only 3.5 MPa·m$^{1/2}$ coupled with a reduced fracture strength.

I. Introduction

SELF-REINFORCED β-silicon nitrides are an analogue to whisker-reinforced ceramics relying on the formation of elongated rodlike grains, which are similar in form to whiskers, to toughen the ceramics.[1] Li and Yamanis[2] demonstrated that silicon nitrides containing large (≥1 μm diameter) elongated grains could exhibit steady-state toughness values approaching 10 MPa·m$^{1/2}$ (as compared to ~3 MPa·m$^{1/2}$ for submicrometer grain size material). Furthermore, bridging of cracks by intact elongated grains and grain pullout are observed in the region behind the crack tips, just as with whisker-reinforced ceramics. In two independent experiments, Kawashima *et al.*[3] and Mitomo *et al.*[4] showed that the fracture toughness of silicon nitride increased with the diameter of the larger elongated grains, consistent with the response predicted for frictional bridging and pullout processes.[5]

Such reinforcements are possible as the β-grains in silicon nitride ceramics generally exist as elongated hexagonal prisms, even in fine-grained materials. The growth of β-grains is anisotropic with the *c*-axis growth rates generally exceeding those normal to the prism faces.[6,7] Such grain growth occurs in the presence of a glass phase derived from the native surface oxide on the silicon nitride powders and additives used to enhance the densification of the silicon nitride ceramics. The additives affect the glass viscosity by altering the glass composition.[8,9] When growth of the β-grains is controlled by diffusion through the glass phase, changes in glass composition modify the diffusion rates of silicon and nitrogen and, thus, the rate of grain growth.[7] In the case of interface-controlled growth of the larger β-grains, it is not clear that the changes in composition within the same glass system would have significant effects on growth rates. On the other hand, substitution of various rare-earth ions can have a significant effect on the growth rates of β-grains.[10] In the earlier study,[10] it was suggested that the growth-limiting step shifted from interface control to control by diffusion within the glass phase as the rare-earth cation decreased in size.

On the other hand, the extent of anisotropic grain growth and the fraction of larger elongated grains can also be manipulated by the ratio of α- to β-phase Si_3N_4 in the starting powders, as well as the sintering temperatures and hold time.[11–13] It is possible to produce an essentially equiaxed β-silicon nitride if the starting powder consists only of β-phase.[12–14] The presence of some β-particles in an α-phase powder is often used to develop a microstructure consisting of larger elongated β-grains in a matrix of finer β-grains and an amorphous or partially crystallized grain boundary phase. In fact, many available powders consist primarily of α-phase with only a few percent β-phase. One can add β-phase powder to alter the fraction of larger elongated grains present in the ceramic. A refinement of this approach is the use of elongated β-seeds.[15,16] This refinement enhances the formation of large elongated β-grains and provides improvements in the control of both the size and the fraction of these larger elongated grains. More recently, size separation of β-phase powder followed by selective additions of the coarser particles to the fines has been used to develop similar reinforced microstructures.[17]

As noted earlier, toughness measurements in silicon nitrides with fixed additive contents (i.e., 5 wt% yttria + 2 wt% alumina) indicated that the steady-state toughness for long cracks increases with the diameter of the larger elongated grains.[3,4] However, the influence of the fraction of large elongated grains and the size of the finer ''matrix'' grain on the rise in fracture resistance with crack extension, as well as on fracture strength, has not been systematically examined. In the past, one typically expected that the fracture strength would decrease with an increase in grain size. Studies of self-reinforced silicon nitrides indicate that the strength can decrease with increase in size of the reinforcing grains while the toughness and resistance to machining damage increase.[18] The resistance to machining

S. M. Wiederhorn—contributing editor

Manuscript No. 190763. Received August 20, 1997; approved March 17, 1998.
*Member, American Ceramic Society.
†Now at Unilever Research, Bedfordshire, England.
#Now at Los Alamos National Laboratory, Los Alamos, New Mexico.

damage may be related to the rising fracture resistance; however, the effect of microstructure on the rise in the fracture resistance with the growth of short cracks has not been adequately addressed. Previous measurements in silicon nitrides indicate that the *R*-curve response can be altered by the size and amount of the larger elongated grains.[19,20] From these studies it appears that a coarsening of the overall microstructure (both the finer matrix grains and the reinforcing grains) may benefit the steady-state (long crack) toughness but only yield a slowly rising *R*-curve. On the other hand, earlier results for whisker-reinforced aluminas reveal that both the amount and diameter of the reinforcing phase could enhance the overall *R*-curve response.[21] Indeed, both the rate of rise with initial crack extension and the steady-state toughness values were increased with the content and diameter of the whiskers. The current study was initiated to compare the effect of microstructure on the rise in fracture resistance with crack extension (*R*-curve) and fracture strength. To this end, samples were prepared that had either essentially equiaxed β-grains (unreinforced) or both different sizes and size distributions of elongated β reinforcing grains. Gas pressure sintering and hot pressing plus seeding with elongated β-particles were employed to control the microstructures achieved.

II. Experimental Procedure

(1) Gas-Pressure-Sintered (GPS) Samples

The β-Si_3N_4 seeds were grown by heating a powder mixture of Si_3N_4, Y_2O_3, and SiO_2 in a silicon nitride crucible at 1850°C for 2 h under a nitrogen pressure of 0.5 MPa, followed by acid rinse treatments. After milling, the seeds were defect-free rod-like β-Si_3N_4 single-crystal particles (~1 μm in diameter by ≥2 μm in length) with very low levels of impurities (0.26% oxygen and 1.3 ppm yttrium). Details of the preparation and characterization of the seeds are reported in Ref. 22. Seeded silicon nitrides were prepared by tape casting, except where noted, and gas pressure sintering. The starting powders were Si_3N_4 (E-10 grade, ≥95% α-phase, Ube Industries, Japan), Y_2O_3 (purity >99.9%, BET 27 m^2/g, Hokko Chemicals, Japan), Al_2O_3 (purity >99.9%, BET 173 m^2/g, Hokko Chemicals, Japan), and 2 vol% β-Si_3N_4 seed particles. Two compositions of densification additives were used: (1) 6.25 wt% Y_2O_3 + 1 wt% Al_2O_3 and (2) 5 wt% Y_2O_3 + 2 wt% Al_2O_3. For comparison, a fine-grain silicon nitride without β-Si_3N_4 seeds was also prepared by cold isostatic pressing powder mixtures and, then, gas pressure sintering. Samples were densified at 1850°C for 6 h under a nitrogen gas pressure of 1 MPa. The processing procedures employed are described in greater detail in Ref. 16. Measurements based on Archimedes' principle showed all the samples were at least 98% of theoretical density (based on theoretical densities of β-Si_3N_4 and the oxynitride glasses) except for the tape cast and sintered composition with 6.25 wt% Y_2O_3 and 1.0 wt% Al_2O_3 that was 94% of theoretical density.

(2) Hot-Pressed Samples

All the materials produced by hot pressing used oxide additives of 1 wt% Al_2O_3 (AKP50, Sumitomo Chemical America Inc.) + 6.25 wt% Y_2O_3 (99.9% purity, Molycorp Inc.) mixed into the silicon nitride powders. Samples were prepared starting with α-Si_3N_4 powder (E-10 grade, ≥95% α-phase, Ube Industries, Japan). Finally, one sample was prepared (using the same oxide additive composition) using a β-Si_3N_4 powder (KSN-80SP, ~90% β-phase, Shin-Etsu Chemical Co., Ltd., Japan) to form an equiaxed silicon nitride.

For these nonseeded samples using α-Si_3N_4 powders, the silicon nitride, yttria + alumina powder mixtures were attrition milled for 3 h in a Teflon-coated mill with 750 g of Si_3N_4 media using a slurry of 250 mL of 2-propanol and 75 g of the powder mixture. The mixture was dried and crushed to pass through 200-mesh sieve. For the nonseeded samples based on the β-Si_3N_4 powder, 75 g of the powder mixture together with 200 mL of 2-propanol was ball-milled for 24 h in polyethylene bottle using 300 g of Si_3N_4 media. Afterward, the mixture was again dried, crushed, and passed through a 200-mesh screen.

All of these samples were fabricated in a hot-press equipped with an extensiometer to measure ram travel using the following cycle. Samples were heated to 1000°C in ~45 min under a vacuum of 1 Pa with no applied load and held at 1000°C for 1 h, and then the chamber was backfilled with nitrogen (0.1 MPa) and a load of ~20 MPa was applied. The temperature was raised to 1750°C in ~30 min and held there for 2 h, the sample was then cooled to 1000°C in ~30 min under load, the load was then removed, and the sample was cooled to room temperature. One sample prepared from a mixture of α-Si_3N_4 powder, 1 wt% Al_2O_3, and 6.25 wt% Y_2O_3 was hot-pressed for only 20 min at 1750°C to produce a self-reinforced material with a finer microstructure. All samples exhibited densities >99% of theoretical regardless of composition.

In addition, two GPS self-reinforced silicon nitride ceramics (SN-1 and SN-2) supplied by NKK Corp. that employed addition of 5 wt% Y_2O_3 + 2 wt% Al_2O_3 to UBE E10 α-Si_3N_4 powder were examined. Earlier studies suggested that these would have toughness and strength values in the range of 5 to 9 $MPa \cdot m^{1/2}$ and 600 to 1000 MPa, respectively.[3]

(3) Characterization

In order to characterize microstructural features, samples were mechanically polished through 0.5 μm diamond abrasive and then plasma etched using a mixture of CF_4 with ~5% oxygen for 2 to 5 min. The samples were then carbon coated and examined in a scanning electron microscope (SEM)[‡] while chemical analysis was accomplished using an energy dispersive spectrometer attachment.[§] Quantitative microstructural analyses (e.g., grain diameters, second phase content) were conducted utilizing analytical software[¶] and the techniques described in Ref. 23. In the present study, three different magnifications (4485×, 7476×, and 29,902× or 37378×) were employed. With each composition, the diameters of 1000 to 1500 grains were measured. The cation concentrations (Al, Y, and Si) were determined from quantification analyses of the EDS spectra. In addition, X-ray diffraction (XRD) analysis was performed to confirm the completion of the α-to-β transformation, as well as to identify any crystalline secondary phases present.

(4) Testing

The *R*-curve response of the composites was measured using an applied moment double cantilever beam (AMDCB) geometry.[24] AMDCB and flexure test specimens were machined using diamond slicing and grinding wheels. AMDCB specimen (10 mm wide × 2.5 mm thick × 35 mm long) contained a 1 mm deep by 1.5 mm wide centerline groove parallel to the length of the sample on one wide (10 mm × 35 mm) surface. The face opposite the grooved side of the AMDCB specimen was mechanically polished (0.5 μm alumina final abrasive) to facilitate observation of the crack. A 1.5 mm wide notch, 8 mm deep, was cut into one end of each sample centered on the 1.5 mm centerline groove. The remaining web at the base of the notched end of each AMDCB sample was cut with a 0.35 mm thick diamond blade to produce a section with a tapered thickness to facilitate precracking of the specimen. Then a line of 3 kg Vickers indentations spaced ~75 μm apart was placed along the centerline on the polished surface starting at a point ~50 μm below the root of the end notch. The line of indentations served to generate a precrack that could be extended in a controlled manner. This was accomplished by pressing a TiB_2

[‡]Hitachi S-4100 field emission gun scanning electron microscope with images recorded either digitally via a 4pi Analysis Inc. spectral engine and scanning interfaced MacIntosh Quadra 840AV computer or video recording. SEM equipped with microshannel plate baskscattered electron detector, GW Electronics, Norcross, GA.

[§]Model 440B-1SPT detector, Noran Instruments with DTSA analytical software from NIST.

[¶]Prism Image Analysis software, Analytical Vision, Inc., Raleigh, NC.

wedge into the end notch of the AMDCB sample. The precrack was extended until the crack tip was well into the region of constant web thickness. Note that in all of the tape cast and sintered materials containing elongated seeds the large elongated grains tended to be oriented in the tape casting direction which is parallel to the polished surface of the AMDCB specimen as discussed in Ref. 25. In the tape cast and sintered samples, AMDCB specimens were prepared with the crack plane oriented with the crack plane perpendicular to the tape casting direction. As noted in the companion paper, there was a small (~10%) reduction in plateau toughness values when the crack plane orientation was changed from being perpendicular to parallel to the tape casting direction due to the texturing of the large elongated grains.[25] The crack tip wake region was then removed with a low-speed diamond saw equipped with a stereo-optical microscope to monitor the crack length. Final crack lengths of 50 to 100 μm could be obtained as determined with an optical microscope using either polarized light or Nomarski phase contrast.

Stainless steel loading arms were then attached to the cleaned and dried AMDCB samples using an epoxy adhesive. Alignment of the loading arms and sample was maintained during curing of the epoxy adhesive in a mounting fixture. After curing the adhesive, the samples were cleaned and tested. Tests were conducted on an AMDCB test module[††] placed on the stage of either the optical microscope[‡‡] (22°C, 50% relative humidity) or the scanning electron microscope. This provided detailed observations while the sample was subjected to selected applied load schedules. The test stage[21] employed a DC drive motor with a worm gear to generate the various applied loading schedules, and the load was monitored by a semiconductor load cell. The *x–y* stages on both microscopes were equipped to allow the *x* and *y* positions to be continuously monitored and acquired to record the crack tip position.

Flexure bars were also prepared, and their surfaces finished with a 400-grit diamond grinding wheel grinding in the direction parallel to the length of the flexure bar. The edges of the bars were chamfered using a 6 μm diamond lapping wheel. In the tape cast GPS samples, the tensile surfaces were parallel to the tape casting surface and the tensile axis was parallel to the tape casting direction. In either the cold-pressed GPS samples and the hot-pressed samples the tensile surfaces were perpendicular to the pressing axis. The cross-sectional dimensions of the flexure bars were typically 4 mm wide by 3 mm thick. Flexure tests were conducted at 22°C in 50% relative humidity at a loading rate of 70 MPa/s using a four-point flexure fixture (inner and outer spans of 20 and 40 mm, respectively) mounted on a universal test machine.[§§]

III. Results

(1) Microstructural Analysis

(A) Grain Size—6.25Y:1A1: Typical microstructures of the silicon nitrides prepared with 6.25 wt% Y_2O_3 + 1 wt% Al_2O_3 are shown in Fig. 1. A distinct bimodal grain size distribution is evident in the micrographs and the analysis of grain diameter distributions (Fig. 2) for both the seeded GPS sample and the nonseeded sample hot-pressed for 0.33 h at 1750°C. In each of these materials, the finer matrix grains have average diameters less than 0.6 μm. Obviously, the intentionally added large β-seeds dominate in the generation of large elongated grains (Fig. 1(a)). Note that the β-cores are accentuated by differential plasma etching of β-Si_3N_4 versus the β′-$Si_{6-z}Al_zO_zN_{8-z}$ growth layer. The formation of a distinct population of elongated grains larger than the matrix grain is evident also when the nonseeded sample is hot-pressed for 0.33 h. In this case, the larger β-particles present in the powder act as seeds to form the larger elongated grains. Here the β-Si_3N_4 cores (arrow, Fig. 1(c)) are observed less frequently as they are much smaller than those in the seeded sample (Fig. 1(a)). Note that full density is attained within 15 min after reaching 1750°C as indicated by the hot-press extensiometer readings. With extension of the hold time during hot pressing, the fraction of large elongated grains increases, accompanied by significant grain growth as seen in Figs. 1(c) versus (b), and Figs. 2(c) versus (b). These results also reveal a significant coarsening of the ''finer'' matrix grains in the nonseeded samples that results in transition to a broad grain diameter distribution as the hold time at temperature is increased. The grains in the sample fabricated from the β-phase powder are essentially equiaxed with an average grain size of ~0.4 μm (Figs. 1(d) and 2(d)). In all cases, β-Si_3N_4 and β-SiAlON were the only crystalline phases detected by XRD.

(B) Grain Size—5Y:2Al: In samples based on 5 wt% Y_2O_3 + 2 wt% Al_2O_3 as additives, the incorporation of elongated β-seeds again produced a fine-grained matrix and a distinctly bimodal grain diameter distribution as compared to the nonseeded sample processed at the same temperature and time conditions (Figs. 3(a) versus (b), Fig. 4(a) versus (b)). In all cases, β-Si_3N_4 and β-SiAlON were, again, the only crystalline phases detected by XRD. The nonseeded GPS sample exhibits a grain diameter distribution that is not distinctly bimodal. However, compared to the distributions in Figs. 2(b) and (c), the distribution in Fig. 4(b) appears to represent a transition from distinctly bimodal to a broad monomodal distribution. Thus, relying on the β-particle size distribution present in the as-received α-Si_3N_4 powder is not an effective means to generate a distinctly bimodal size distribution. On the other hand, a recent study revealed that the development of a distinctly bimodal powder particle size distribution can be used to generate a well-defined bimodal grain diameter distribution in dense silicon nitrides.[17]

The microstructures of the SN-1 and SN-2 samples are shown as well in Fig. 3. The gas pressure sintering temperature and times are not known specifically; however, based on an earlier paper (Ref. 26), one can deduce that the sintering temperature of the finer-grained material (SN-1) was 1750° to 1800°C and that of the coarse-grained material (SN-2) was 1950° to 2000°C. Neither sample exhibits a distinct bimodal distribution of grain diameters; rather, both exhibit a broad grain diameter distribution (Figs. 4(c) and (d)). The largest grains in the coarse-grained, SN-2, material are somewhat greater than those in the seeded GPS sample. However, the major difference is in the much finer matrix grain size in the seeded GPS sample together with a more uniform dispersion of a smaller fraction of the larger elongated grains.

(C) Compositional Characteristics: In systems containing aluminum, grain growth is accompanied by the incorporation of Al and O into a β′-$Si_{6-z}Al_zO_zN_{8-z}$ layer[27] that forms on the β-Si_3N_4 core. This is evidenced by the different etching rates between the β-Si_3N_4 core and the β′-$Si_{6-z}Al_zO_zN_{8-z}$ outer shell (Figs. 1 and 3). As might be expected, chemical analysis shows that the growth region of the large reinforcing grains contains, on average, more Al with increase in Al content in the additives.[25,28] It is also found that the aluminum content decreases when traversing from near the core to the outer region of the β′-$Si_{6-z}Al_zO_zN_{8-z}$ layer of the large reinforcing grains. For each composition, the β′-$Si_{6-z}Al_zO_zN_{8-z}$ in each growth layer exhibits a maximum *z*-value between 0.05 to 0.1 in the region where it first epitaxially deposits onto the β-Si_3N_4 core and then decreases near the interface with the glass phase.[25] In the large elongated grains produced by intentional seeding, the aluminum content is generally less than that in the grains in the nonseeded samples. In the seeded GPS samples, the aluminum content of the retained glass phase decreases with an increase in the initial Y_2O_3:Al_2O_3 ratio in the densification additives. Finally, an increase in the Y:Al ratio in the retained glass is

[††]Fabricated by Raith USA, Inc., Farmingdale, NY.
[‡‡]Nikon HU-11 Toolmakers microscope with polarized light and Nomarski phase contrast features. Image recorded via either computer interface or video recording.
[§§]Instron 1122 universal test machine.

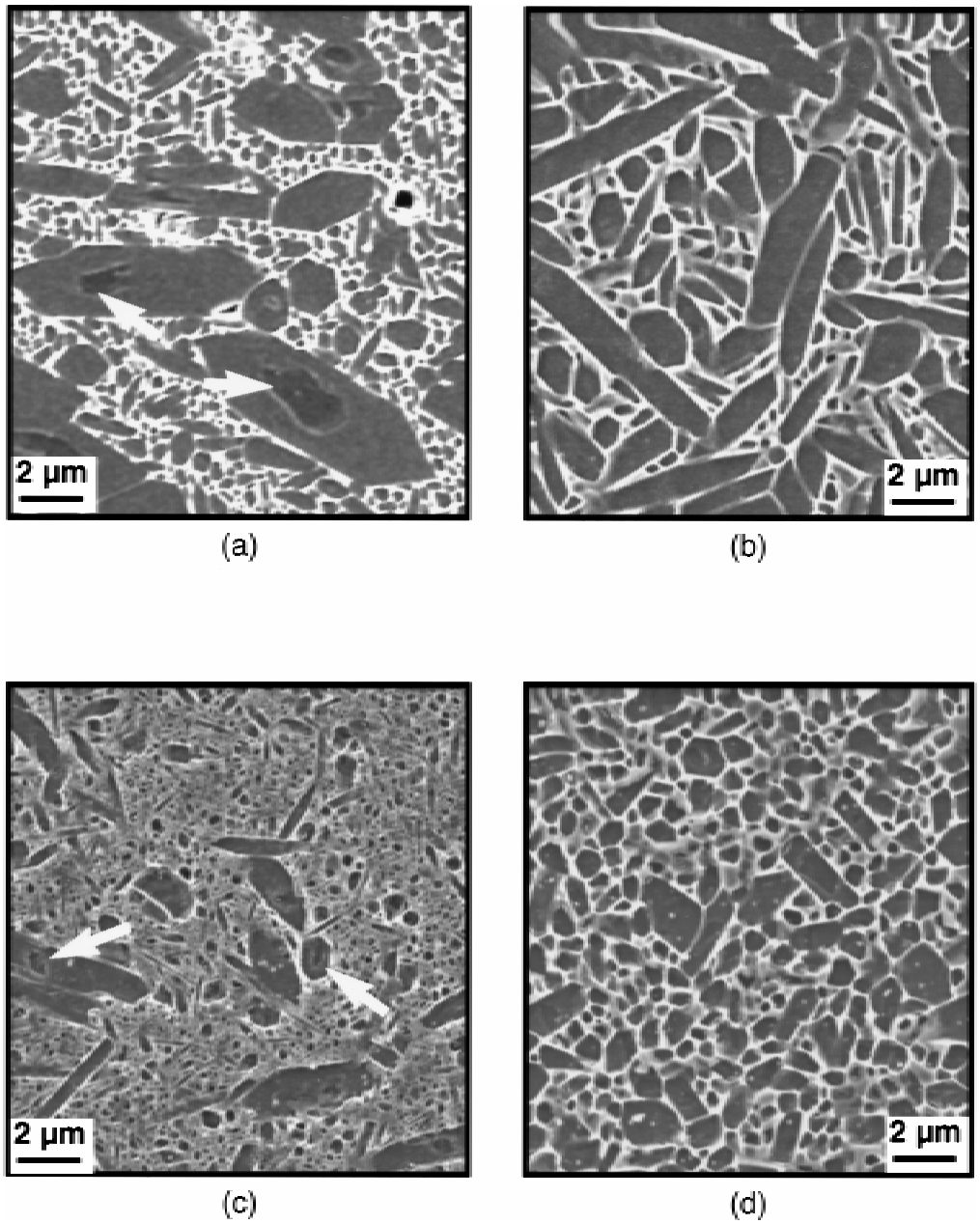

Fig. 1. Microstructures of silicon nitrides using a mixture of 6.25 wt% yttria + 1 wt% alumina as a densification additive: (a) 2 wt% elongated β-seeds, gas pressure sintered at 1850°C for 6 h, UBE E-10 α-powder; (b) no elongated seeds, hot-pressed at 1750°C for 2 h, UBE E-10 α-powder; (c) no elongated seeds, hot-pressed at 1750°C for 0.33 h, UBE E-10 α-powder; (d) no elongated seeds, hot-pressed at 1750°C for 2 h, ShinEtsu β-powder. Plasma etching highlights the β'-$Si_{6-z}Al_zO_zN_{8-z}$ growth layer on the β-Si_3N_4 cores (arrowed) in these SEM micrographs.

noted due to the incorporation of Al into the β'-$Si_{6-z}Al_zO_zN_{8-z}$ growth layer on the β-Si_3N_4 cores.

(2) Fracture Resistance and Flexure Strength Response

(A) 6.25Y:1Al: These experiments represent a more extensive examination of the influence of grain shape and size on the fracture resistance. The data in Fig. 5 illustrate that there is a strong effect of microstructure on the room-temperature fracture resistance curves in the materials fabricated using the mixture of 6.25 wt% yttria + 1 wt% alumina as sintering additives. In the nearly equiaxed material (d), one can see that the steady-state toughness is only 3.5 MPa·m$^{1/2}$ and that the fracture resistance should fall below 2 MPa·m$^{1/2}$ for crack lengths <100 μm. On the other hand, the introduction of large elongated grains clearly increases the steady-state fracture resistance. Comparison of the results for the GPS seeded material to the nonseeded material hot-pressed for only 0.33 h, where the number of the larger elongated grains are comparable, indicates that the steady-state toughness increases with the diameter of the larger elongated (and matrix) grains. When the nonseeded material is hot-pressed for 2 h, the toughness increases as compared to the material hot-pressed at the shorter time. In this case though, both the overall grain size distributions and the number of larger elongated grains are increased. In each case the magnitude of the fracture resistance values in the initial rising portion of the *R*-curves increases with the steady-state toughness level. For the tougher materials, the initial portion of the *R*-curve appears to be extremely steep. The incorporation of the larger β-seeds to generate the larger elongated grains combined with a fine matrix grain size appear to be the most effective method to enhance the *R*-curve response.

At this point, one still cannot discern how or whether the

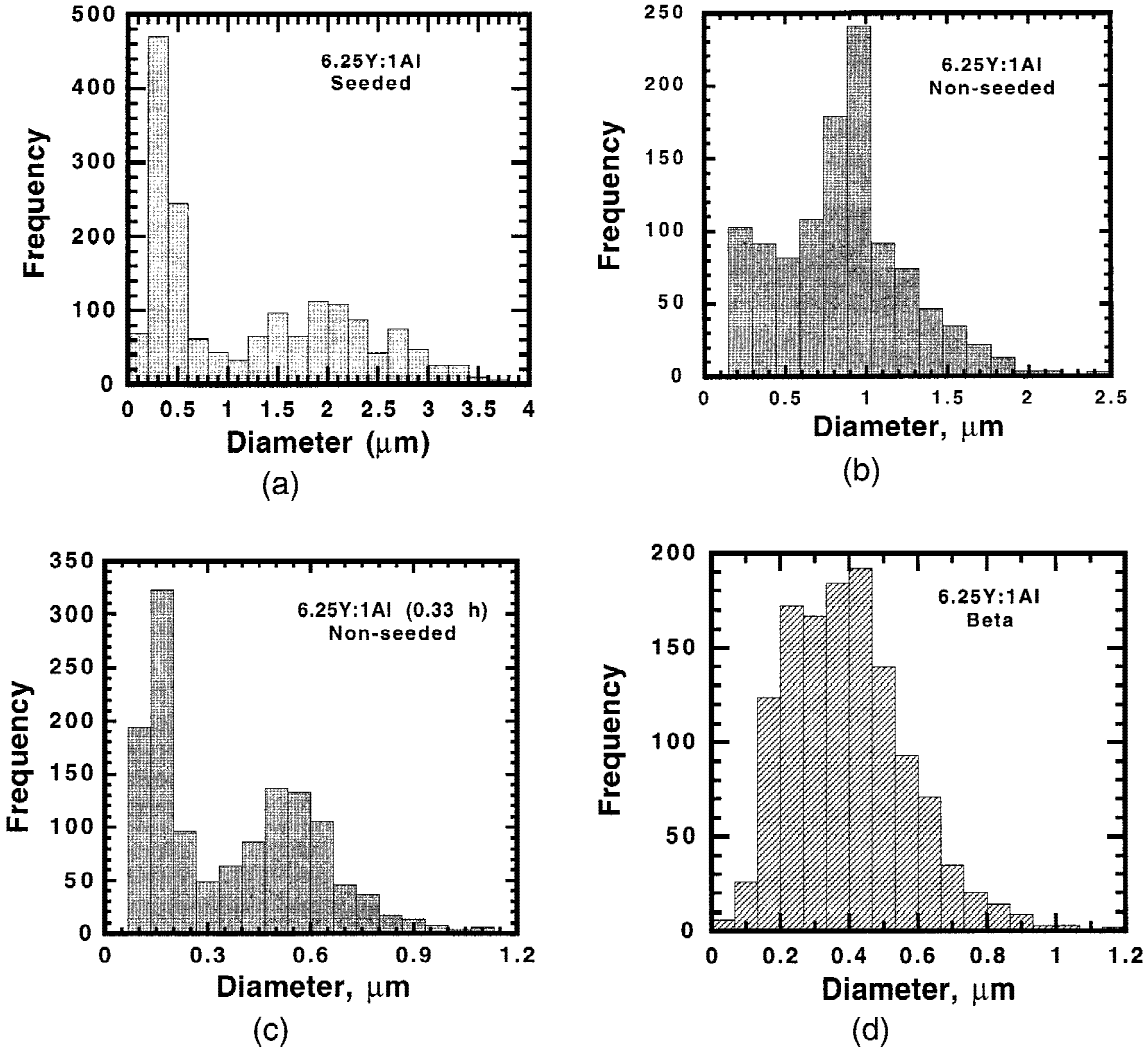

Fig. 2. Grain diameter distributions are altered by seeding and by densification conditions as noted in the silicon nitrides that employed 6.25 wt% yttria + 1 wt% alumina additions (see corresponding micrographs in Fig. 1).

fracture resistance values for crack lengths approaching zero are significantly modified by the different microstructures. However, earlier studies of whisker-reinforced fine-grained aluminas indicate that such microscopic rodlike reinforcements also cause crack deflection which raises the intercept fracture resistance value.[29] Obtaining meaningful fracture resistance values for crack lengths less than 50 μm in length are a subject of concern. Thus, we can only suggest that increases in the fraction of the larger elongated grains should enhance crack deflection and raise the intercept value of the fracture resistance.

The generation of a fine-grained matrix coupled with well-dispersed large elongated grains has a dramatic effect on the fracture strength of these silicon nitride ceramics (Table I). Samples with diamond-ground (400-grit) surfaces from the seeded GPS material with a distinctly bimodal grain diameter distribution with submicrometer matrix grains exhibit strengths >1 GPa. The very fine-grained nonseeded silicon nitride also reaches the fracture strengths ~1 GPa, but this is coupled with a low fracture toughness. Without the development of a bimodal size distribution, grain growth reduces the fracture strength.

(B) 5Y:2Al: Figure 6 illustrates the *R*-curves for the silicon nitride ceramics based on a mixture of 5 wt% yttria + 2 wt% alumina as densification additives. The material fabricated using the elongated β-seeds (curve 6(a)) again exhibits both the highest steady-state toughness and the most rapidly rising fracture resistance with the extension of the short cracks. The finer microstructure of the nonseeded GPS sample (curve 6(b)), together with a less well-defined bimodal size distribution, reduces the steady-state toughness as compared to the seeded sample. However, the fracture resistance of this relatively fine-grained nonseeded material quickly reaches its steady-state level (i.e., at crack lengths of <500 μm). Conversely, both the fine-grained SN-1 (curve 6(d)) and coarse-grained SN-2 (curve 6(c)) samples without the bimodal grain diameter distributions have more gradual increases in fracture resistance with extension of the short cracks. However, the increase in the diameter of the larger elongated grains in SN-2 does raise the highest steady-state toughness as compared to that of SN-1. A rapid increase in fracture resistance with crack extension in a silicon nitride ceramic with a bimodal grain diameter distribution of this same composition was also observed by Ohji *et al.*[20] This provides additional support of the use of well-dispersed large elongated grains in a fine-grained matrix for enhancing the *R*-curve response.

Finally, the fracture strengths are strongly affected by the microstructural scale in this composition as well (Table I). A fine (submicrometer) grained matrix containing well-dispersed large elongated grains yielded exceptional fracture strengths with values ≥1 GPa achieved in samples with 400-grit diamond ground surface finishes. Reducing the grain size range while retaining a bimodal size distribution of grain diameters only resulted in strengths approaching 950 MPa in nonseeded samples. In all materials with broad monomodal grain diameter distributions, the fracture strengths were decreased significantly.

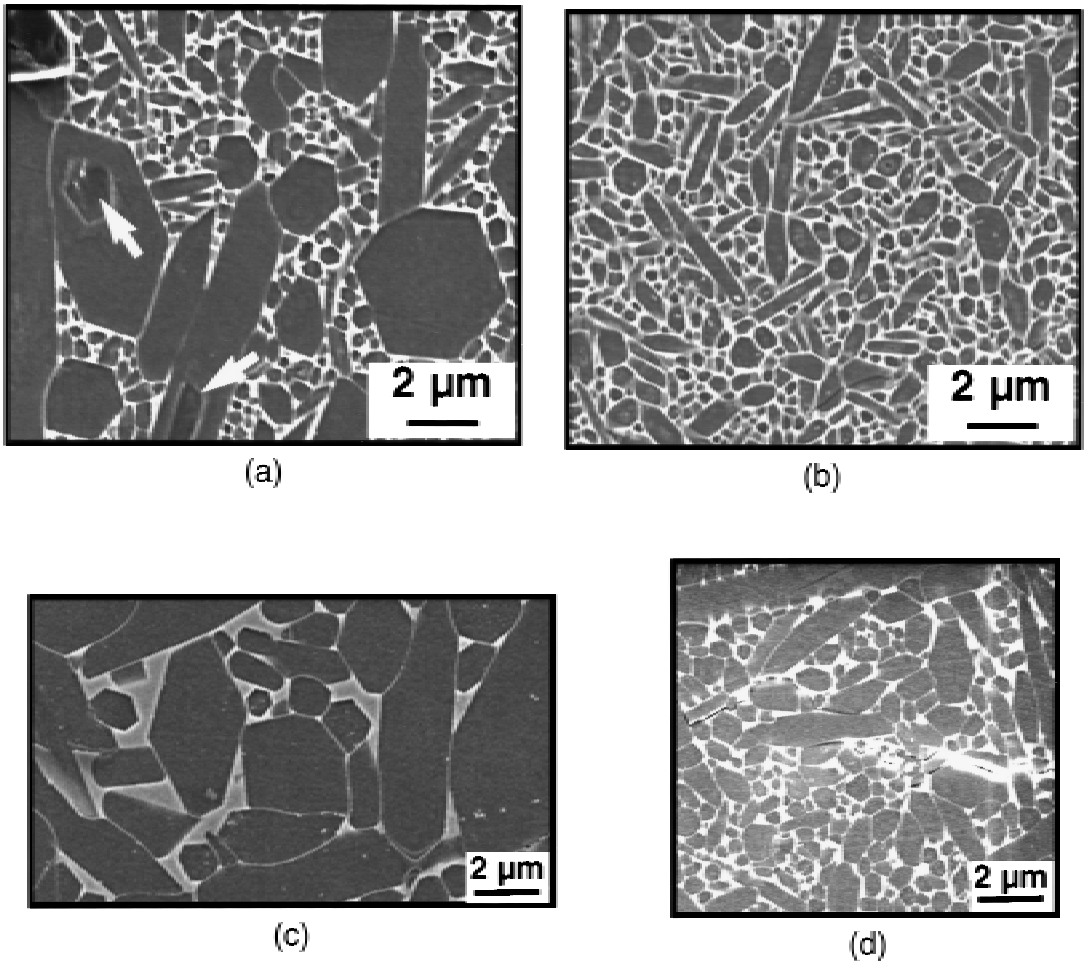

Fig. 3. Microstructures of silicon nitrides densified using an additive mixture of 5 wt% yttria + 2 wt% alumina: (a) seeded tape cast, gas pressure sintered at 1850°C for 6 h, UBE E-10 α-powder; (b) not seeded, cold-pressed, gas pressure sintered at 1850°C for 6 h, UBE E-10 α-powder; (c) SN-2 coarse-grained ceramic; (d) SN-1 fine-grained ceramic.

IV. Discussion

(1) Microstructural Control

The control of the microstructural development in the present materials utilized elongated β-seeds added into α-phase powder. The much larger sized elongated β-seeds dominated the grain growth process and established the fraction of large elongated grains. In fact, earlier studies using the same approach showed that the fraction of larger elongated grains in the sintered samples is a direct function of the original content of the elongated β-seeds.[16] In the seeded materials examined here, the bimodal size distribution was maintained in samples of the same composition whether hot-pressed at 1750°C for 2 h, gas pressure sintered at 1850°C for 6 h, or annealed at 1875°C for 5 h after gas pressure sintering.[30] The mean value of the grain diameters of both the fine-grained matrix and the large reinforcing grains simply increased with temperature (and time). In contrast, the growth rate of the layer formed on the elongated cores during gas pressure sintering at 1850°C for 6 h was not very sensitive to changes in additive composition and glass-phase composition. Under these conditions, the glass viscosity and, hence, diffusion through the glass must be quite similar in these two compositions. This is supported by data for the bulk SiAlYON glasses where the transition and softening points all lie within ±25°C over a wide range of composition.[8,9]

Using a 95% α-powder and no intentionally added seeds, a bimodal size distribution is also observed immediately after full density is achieved by hot pressing at 1750°C for 0.33 h. However, the size range of β-grains generated at this point must be reasonably broad as numerous additional larger elongated grains are generated as the hold time at 1750°C is increased. The microstructures of the SN-1 and SN-2 GPS materials exhibit a similar broad range of grain diameters. Clearly, seeding with larger β-particles is required if one wishes to generate a controlled microstructure with a distinctly bimodal size distribution.

Grain growth in the presence of aluminum-bearing additives is accomplished by the generation of a β'-$Si_{6-z}Al_zO_zN_{8-z}$ layer on existing β-grains. In the present case, these growth layers are composed of low z-value material, typically $z \leq 0.1$, and continued growth results in depletion of the aluminum content of the glass phase. This process results in a β'-$Si_{6-z}Al_zO_zN_{8-z}$ growth layer that exhibits a decrease in aluminum content, and z-value, from the interface with the core to the interface with the glass phase. Earlier studies showed that β'-$Si_{6-z}Al_zO_zN_{8-z}$ growth layers on whiskers inhibited interfacial debonding pertinent to toughening by elongated grains that bridge the crack.[31] However, very detailed studies of these same samples (in Ref. 31) reveal that there is a gradient in oxygen content which rises from a low (but nonzero) value in the silicon nitride close to the interface to a high value in the glass even in the sample where a SiAlON growth layer had not been detected earlier.[28] This recent observation suggests that interface debonding is not simply a function of the presence or absence of a SiAlON growth layer but also by the oxygen (and Al content) of the layer. The toughening effects of the formation of elongated grain might be enhanced, then, by controlling the composition of the β'-$Si_{6-z}Al_zO_zN_{8-z}$ growth layer. This is the subject of a companion paper.[25] One should consider these

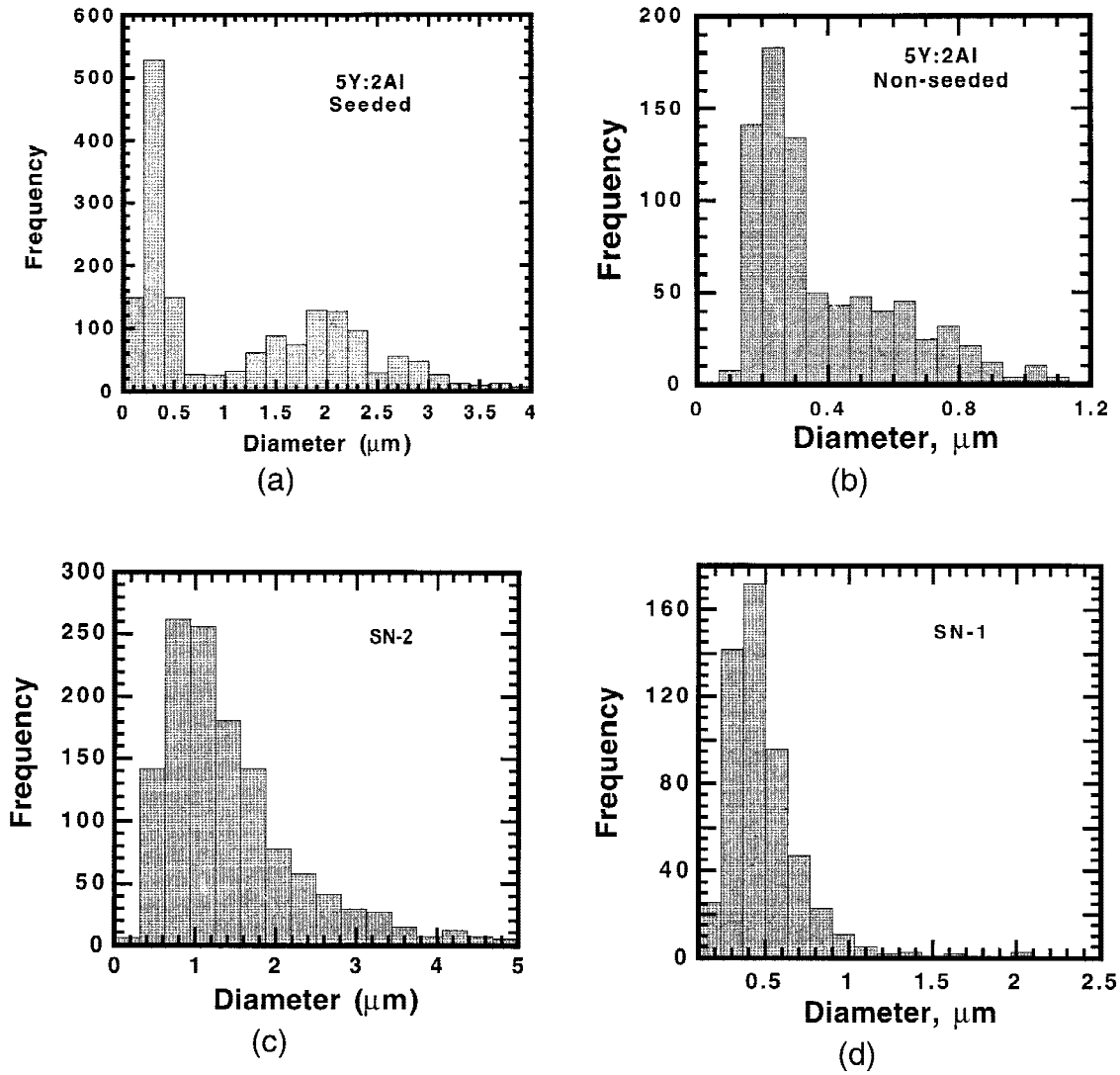

Fig. 4. Grain diameter distributions are altered by seeding and by densification conditions as noted in the silicon nitrides that employed 5 wt% yttria + 2 wt% alumina additions (see corresponding micrographs in Fig. 3).

effects as additional grain growth will continuously reduce the *z*-value of the growing β'-$Si_{6-z}Al_zO_zN_{8-z}$ layer and, in turn, modify interfacial debonding and toughening effects. Thus increasing the diameter of the elongated grains to enhance crack bridging contributions to the toughness can be accompanied by increased contributions from interfacial debonding as the grains grow and decrease the *z*-value of the growth layer.

(2) Effects of Microstructure on the R-Curve Response

Increasing the size of the reinforcing grains will enhance contributions from both frictional bridging and pullout. In addition, enhancing interfacial debonding, the number of bridging reinforcements, and the length of the debonded interfaces should result in a more rapid rise in the *R*-curve as well as high toughness.[21] The increase in the rising fracture resistance behavior as the bimodal grain diameter distribution shifts to larger sizes (curves a and c in Fig. 5) reflects the contribution of bridging processes. The effect of crack bridging by the larger elongated grains is emphasized when the *R*-curve for the fine equiaxed material (curve d in Fig. 5) is considered. In this case, the *R*-curve rises very slowly, reaching a steady-state value of only 3.5 $MPa \cdot m^{1/2}$. This is consistent with a very negligible crack bridging contribution as expected when the grains are very small and essentially equiaxed. The transition in *R*-curve response from curves d to c to b to a in Fig. 5 may well reflect an increasing contribution from crack bridging due to increases in the diameter of the reinforcing grains. Similarly, there is a significant enhancement of the *R*-curve with the addition of elongated seeds in the 5Y:2Al composition (curve a versus curve b in Fig. 6).

The generation of a distinctly bimodal microstructure, especially one with the large elongated grains well dispersed in a fine, submicrometer grain sized matrix, is an important factor in optimizing both the fracture resistance and the fracture strength. Materials with a broad grain diameter distribution that incorporate a large fraction of large elongated grains (e.g., material b in Figs. 2 and 5 and the SN-1 and SN-2 samples) exhibit only modest increases in toughness together with much lower strengths. The loss in strength appears to be aggravated by generation of clusters of the large grains (Fig. 7(a)) that are not detected in the high-strength materials (Fig. 7(b)). Earlier observations in similar silicon nitride ceramics also show that clusters of large grains serve as a fracture origin.[10] Finally, a previous study of the effects of the diamond grit size (varied from 1500 to 140 grit) of the surface finishing wheel revealed that silicon nitrides with low toughness values exhibited a substantial loss in strength as the diamond particle size was increased.[18] Increasing the toughness increased the resistance of the material to damage introduced by increasing the diamond particle size. Materials with *R*-curves that rise rapidly to high values at small crack lengths could be expected to be resistant to such damage. Such enhanced damage resistance would be

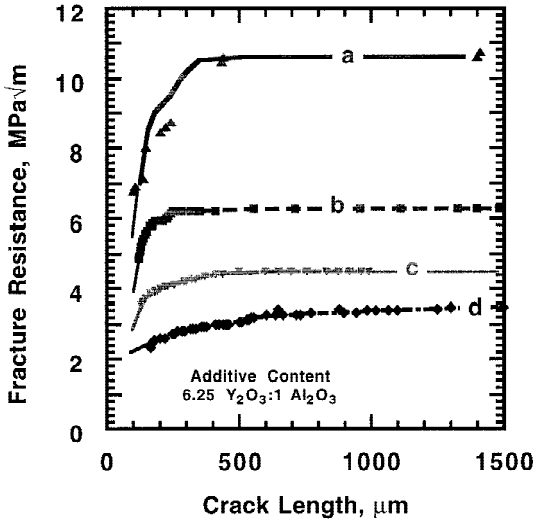

Fig. 5. *R*-curve response for silicon nitride ceramics fabricated using a mixture of 6.25 wt% yttria + 1 wt% alumina as a densification additive. Microstructures a (GPS/seeded), b (HP, nonseeded), c (HP–0.33 h, nonseeded), and d (HP, b) in Fig. 1 correspond to *R*-curves labeled a, b, c, and d.

consistent with the response of all but one of the materials (the hot-pressed fined-grained self-reinforced material with the high yttria to alumina ratio in the additives c in Table I).

It is less clear how the broad grain diameter distribution would result in a more gradually rising *R*-curve, as suggested by the observations in the SN-1 and SN-2 materials. Earlier modeling efforts indicated that a strong contribution from frictional bridging by partially debonded reinforcements should generate a rapidly rising *R*-curve during the initial extension of a short crack.[21] On the other hand, the *R*-curve is predicted to rise at a much slower rate when pullout is the only crack bridging contribution. A large frictional bridging zone behind the crack tip is enhanced by reinforcements with very high fracture strengths or by increasing numbers of reinforcements that participate in the zone. However, an increase in the fraction of large elongated grains also results in numerous grain impingements. These impingements often reduce the grain diameter locally forming notchlike features that could reduce the strength of the reinforcing grain (e.g., Fig. 3(c)). Lower strength for larger versus small diameter elongated grains was suggested in an earlier study of self-reinforced silicon nitrides.[32] In addition, the length of the large elongated grains will be reduced by impingement when the number of such grains increases, except when they are uniaxially aligned. This could serve to reduce the potential length for the interfacial debonding and reduce the efficiency of load transfer from fiber to matrix.[33] These factors should each diminish both the size and the effectiveness of the frictional bridging zone and result in a slowly rising *R*-curve.

This is supported by microscopy observations in the crack tip wake that show the materials with a broad grain diameter distribution involving large grains exhibit little evidence for grain bridging on the surface or the interior (Figs. 8(a) and (b)). In addition, the crack tends to travel along favorably oriented large grain faces with little interaction with these large elongated grains. When large elongated grains are well dispersed in a fine-grained matrix, there is ample evidence of grain bridging (Figs. 8(b) and (c)). Interestingly, protrusion of the fine matrix grains is very evident, indicating a significant contribution to crack bridging by the fine-grained matrix.

As discussed in a companion paper, increases in the aluminum content of the SiAlON growth layer on the reinforcing grains can diminish the toughening response.[25] As noted, the aluminum content of the growth region does change with original additive composition and with the nature of the microstructure. Therefore, the reduced toughness of the nonseeded samples may also reflect the apparent increase in aluminum content in the outer SiAlON layer formed during grain growth.

It is apparent that, at this point, one cannot yet determine the influence of microstructure (and composition) on the fracture resistance values for crack lengths well below 50 μm in these materials. We reiterate that deflection of the crack tip by the reinforcing grains should raise the resistance of the material to advancement of the crack tip. This would have the effect of increasing the intercept value of the *R*-curve. Therefore, we can, at least, indicate that the *R*-curves for the different microstructures will vary. The results for the materials in Fig. 6 are particularly pertinent as one might expect that the larger fraction of larger elongated grains in the SN-1 material would enhance crack deflection and thus have a higher intercept value. Furthermore, the increase in reinforcing grains for the materials tested in Fig. 5 should result in increasing the intercept values of their *R*-curves.

V. Conclusions

High fracture resistance (>10 MPa·m$^{1/2}$) combined with a steeply rising *R*-curve and high fracture strength (>1 GPa) can be developed in self-reinforced silicon nitrides by careful control of the size and amount of well-dispersed large elongated grains in a fine-grained matrix. If not regulated, a microstructure with a broad grain diameter distribution tends to form. If large elongated grains are present, increased fracture resistance can be achieved but is less than that achieved when the techniques such as seeding are used to develop a reinforced microstructure with a distinct bimodal grain diameter distribution. In addition, there is a significant reduction in strength when microstructures consisting of a broad grain diameter distribution

Table I. Room-Temperature Flexure Strengths of Silicon Nitride Ceramics with 400-Grit Diamond Ground Surface Finishes†

Material designation	Average grain diameter	Elongated β-seeds used	Fracture strength (MPa)
	6.25 wt% Y_2O_3 + 1 wt% Al_2O_3		
(a) Fine-grained, reinforced, gas pressure sintered	0.3 μm/2 μm, distinctly bimodal	Yes	1144 ± 126
(b) Medium-grained, reinforced, hot-pressed	~1 μm, broad monomodal	No	850 ± 75
(c) Fine-grained, reinforced, hot-pressed	~0.2 μm/~0.5 μm, distinctly bimodal	No	925 ± 75
(d) Equiaxed, β powder, hot pressed	~0.4 μm, monomodal	No	660 ± 165
	5 wt% Y_2O_3 + 2 wt% Al_2O_3		
(a) Fine-grained, reinforced, gas pressure sintered	10.3 μm/2 μm, distinctly bimodal	Yes	1011 ± 78
(b) Fine-grained, reinforced, gas pressure sintered	0.3 μm/''0.6'' μm, nearly bimodal	No	935 ± 90
(c) SN-2, gas pressure sintered	~1 μm, monomodal with very long tail to larger sizes	No	645 ± 30
(d) SN-1, gas pressure sintered	0.5 μm, monomodal with definite tail to larger sizes	No	660 ± 20

†Resinoid bonded wheel, grinding direction parallel to tensile axis of flexure bars.

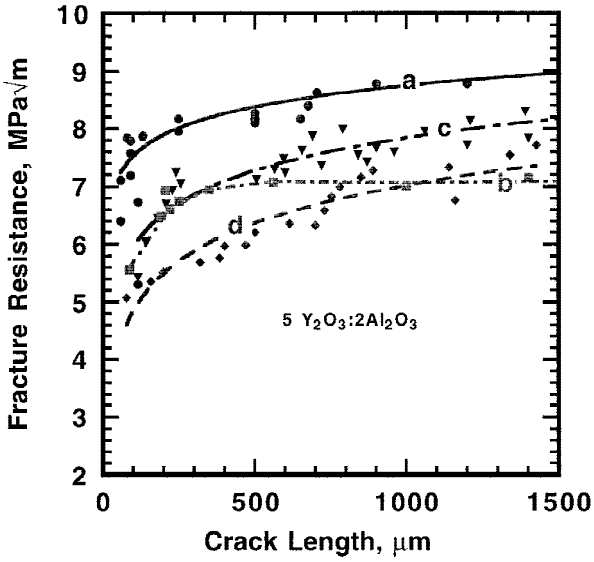

Fig. 6. Rising fracture resistance behavior for silicon nitrides densified using an additive mixture of 5 wt% yttria + 2 wt% alumina. Microstructures a (GPS, seeded), b (GPS, nonseeded), c (GPS, SN-2), and d (GPS, SN-1) in Fig. 3 correspond to *R*-curves labelled a, b, c, and d.

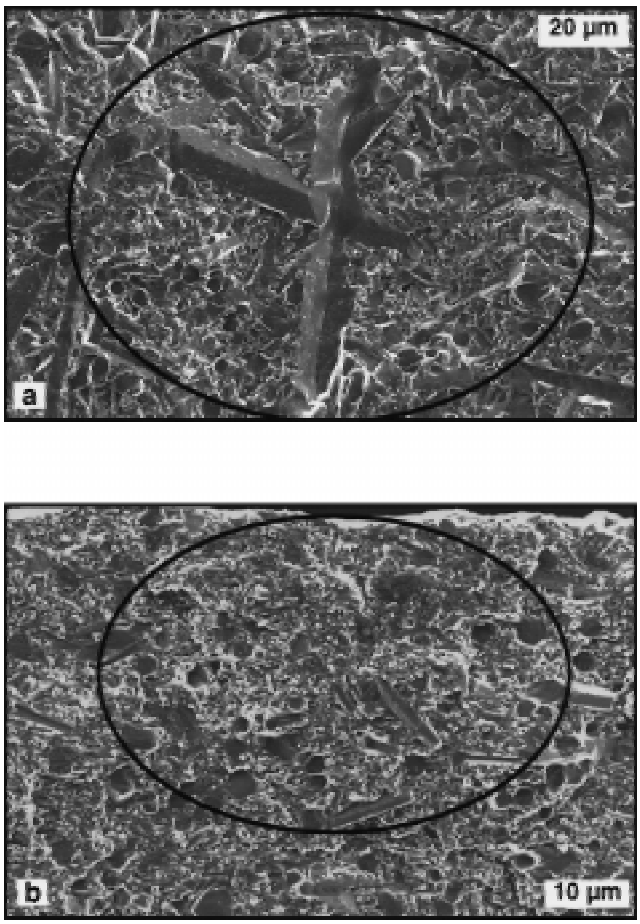

Fig. 7. Fracture origins in self-reinforced silicon nitrides with (a) clusters of large reinforcing grains (low-strength SN-2 material) and (b) with dispersed reinforcing grains (high-strength seeded 5Y:2Al sample).

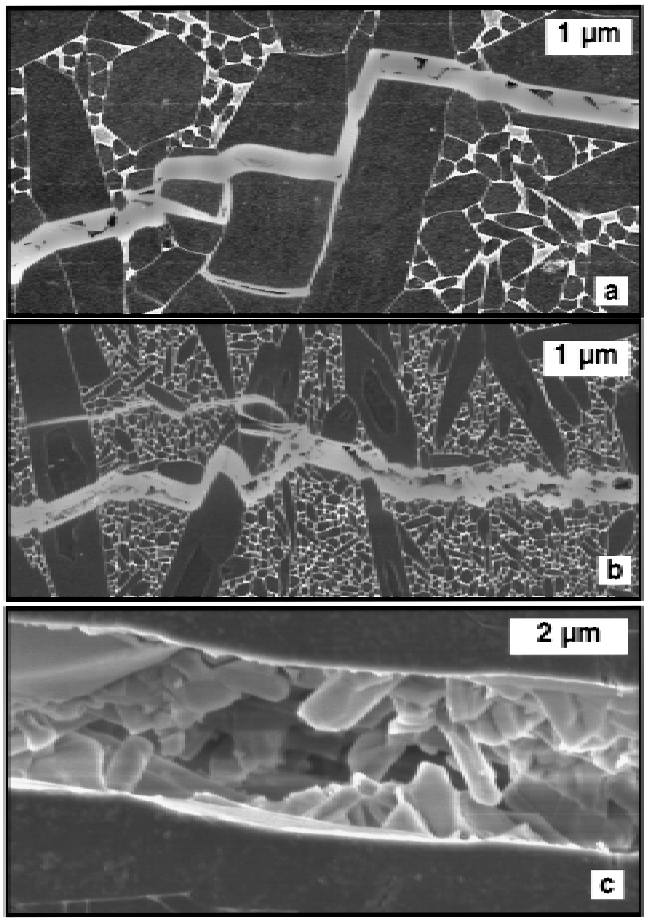

Fig. 8. The extent of bridging by fine, as well as large, elongated grains is noted in silicon nitrides densified with a combination of 5 wt% yttria + 2 wt% alumina ((a) SN-2 coarse-grained sample and (b) seeded GPS sample) and in the seeded GPS sample containing 6.25 wt% yttria + 1 wt% alumina.

are generated. When a fine equiaxed microstructure is generated, both the fracture strength and the fracture resistance are reduced. A steady-state toughness of ~3.5 MPa·m$^{1/2}$ accompanied by a slowly rising *R*-curve response was observed in the unreinforced silicon nitride in the present study.

Acknowledgments: The MITI agency for International Science and Technology Fellowship (Japan) is thanked for supporting K.P.P.'s travel and stay at NIRI–Nagoya to process silicon nitride ceramics. We are also grateful for the efforts of Prof. D. E. Wittmer, Southern Illinois University, in supplying some of the β-Si_3N_4 seed material, Dr. S. Torizuka, Materials and Processing Research Center of NKK Corp., for supplying two self-reinforced silicon nitride ceramics, and Drs. S. D. Nunn and M. K. Ferber in reviewing the manuscript. The research was supported by the Division of Materials Sciences, U.S. Department of Energy, under Contract No. DE-AC05-96OR22464 with Lockheed Martin Energy Research Corp.

References

[1]E. Tani, S. Umebayashi, K. Kishi, and K. Kobayashi, ''Gas-Pressure Sintering of Si_3N_4 with Concurrent Addition of Al_2O_3 and 5 wt% Rare Earth Oxide: High Fracture Toughness Si_3N_4 with Fiber-Like Structure,'' *Am. Ceram. Soc. Bull.*, **65** [9] 1311–15 (1986).

[2]C. W. Li and J. Yamanis, ''Super-Tough Silicon Nitride with *R*-Curve Behavior,'' *Ceram. Eng. Sci. Proc.*, **10** [7–8] 632–45 (1989).

[3]T. Kawashima, H. Okamoto, H. Yamamoto, and A. Kitamura, ''Grain Size Dependence of the Fracture Toughness of Silicon Nitride Ceramics,'' *J. Ceram. Soc. Jpn.*, **99**, 1–4 (1991).

[4]M. Mitomo, ''Toughening of Silicon Nitride Ceramics by Microstructural Control''; pp. 101–107 in *Proceedings of an International Symposium on the Science of Engineering Ceramics*. Edited by S. Kimura and K. Niihara. Ceramic Society of Japan, Tokyo, Japan, 1991.

[5]P. F. Becher, ''Microstructural Design of Toughened Ceramics,'' *J. Am. Ceram. Soc.*, **74**, 255 (1991).

[6](a) M. Krämer and M. J. Hoffmann, ''Grain Growth Studies of Silicon Nitride Dispersed in an Oxynitride Glass,'' *J. Am. Ceram. Soc.*, **76** [11] 2778–84 (1993). (b) M. Krämer, M. J. Hoffmann, and G. Petzow, ''Grain Growth Kinetics of Si_3N_4 During α/β-Transformation,'' *Acta Metall.*, **41** [10] 2939–47 (1993).

[7]C. J. Hwang and T. Y. Tien, ''Microstructural Development in Silicon Nitride Ceramics,'' *Mater. Sci. Forum*, **47**, 84–109 (1989).

[8]E. Y. Sun, P. F. Becher, S. L. Hwang, S. B. Waters, G. M. Pharr, and T. Y. Tsui, ''Properties of Silicon–Aluminum–Yttrium Oxynitride Glasses,'' *J. Non-Cryst. Solids*, **208**, 162–69 (1996).

[9]H. Lemercier, T. Rouxel, D. Fargeot, Jean-Louis Besson, and B. Piriou, ''Yttrium SiAlON Glasses: Structure and Mechanical Properties-Elasticity and Viscosity,'' *J. Non-Cryst. Solids*, **201**, 128–45 (1996).

[10](a) M. J. Hoffmann, ''Analysis of Microstructural Development and Mechanical Properties of Si_3N_4 Ceramics''; pp. 59–72 in *Tailoring of Mechanical Properties of Si_3N_4 Ceramics*. Edited by M. J. Hoffmann and G. Petzow. Kluwer Academic Publishers, Dordrecht, Netherlands, 1994. (b) M. Kanamaru, ''Investigation of Grain Growth in Si_3N_4 Ceramics Containing Rare Earth Oxides'' (in Ger.); Dissertation. University of Stuttgart and Max-Planck-Institute for Metals Research, Stuttgart, Germany, 1994.

[11]S.-M. Han and S.-J. L. Kang, ''Grain Growth in Si_3N_4-Based Materials,'' *MRS Bull.*, **20** [2] 33–37 (1995).

[12]D. D. Lee, S. J. L. Kang, G. Petzow, and D. N. Yoon, ''Effect of α to β (β′) Phase Transition on the Sintering of Silicon Nitride Ceramics,'' *J. Am. Ceram. Soc.*, **73** [3] 767–69 (1990).

[13]W. Dressler, H. J. Kleebe, M. J. Hoffmann, M. Rühle, and G. Petzow, ''Model Experiments Concerning Abnormal Grain Growth in Silicon Nitride,'' *J. Eur. Ceram. Soc.*, **16**, 3–14 (1996).

[14]M. Mitomo, N. Hirosaki, and H. Hirotsuru, ''Microstructural Design and Control of Silicon Nitride Ceramics,'' *MRS Bull.*, **20** [2] 38–41 (1995).

[15]D. E. Wittmer, D. Doshi, and T. E. Paulson, ''Development of Self-Reinforced Composites,'' *Ceram. Eng. Sci. Proc.*, **13** [9–10] 907–17 (1992).

[16]K. Hirao, T. Nagaoka, M. E. Brito, and S. Kanzaki, ''Microstructural Control of Silicon Nitride by Seeding with Rodlike β-Silicon Nitride Particles,'' *J. Am. Ceram. Soc.*, **77** [7] 1857–62 (1994).

[17]H. Emoto and M. Mitomo, ''Control and Characterization of Abnormally Grown Grains in Silicon Nitride Ceramics,'' *J. Eur. Ceram. Soc.*, **17** [4] 797–804 (1997).

[18]Y. Tajima and K. Urashima, ''Improvement of Strength and Toughness of Silicon Nitride Ceramics''; pp. 101–109 in *Tailoring of Mechanical Properties of Si_3N_4 Ceramics*. Edited by M. J. Hoffmann and G. Petzow. Kluwer Academic Publishers, Dordrecht, Netherlands, 1994.

[19]C. W. Li, D. J. Lee, and S. C. Lui, ''*R*-Curve Behavior and Strength for In-Situ Reinforced Silicon Nitrides with Different Microstructures,'' *J. Am. Ceram. Soc.*, **75** [7] 1777–85 (1992).

[20]T. Ohji, K. Hirao, and S. Kanzaki, ''Fracture Resistance Behavior of Highly Anisotropic Silicon Nitride,'' *J. Am. Ceram. Soc.*, **78** [11] 3125–28 (1995).

[21]P. F. Becher, C. H. Hsueh, K. B. Alexander, and E. Y. Sun, ''Influence of Reinforcement Content and Diameter on the *R*-Curve Response in SiC-Whisker-Reinforced Alumina,'' *J. Am. Ceram. Soc.*, **79** [2] 298–304 (1996).

[22]K. Hirao, A. Tsuge, M. E. Brito, and S. Kanzaki, ''Preparation of Rod-like β-Si_3N_4 Single Crystal Particles,'' *J. Ceram. Soc. Jpn., Int. Ed.*, **101** [9] 1051–53 (1993).

[23]J. C. Russ, *The Image Processing Handbook*, 2nd ed. CRC Press, Ann Arbor, MI, 1994.

[24]S. W. Freiman, D. R. Mulville, and P. W. Mast, ''Crack Propagation Studies in Brittle Materials,'' *J. Mater. Sci.*, **8** [11] 1527–33 (1973).

[25]E. Y. Sun, P. F. Becher, C. H. Hsueh, K. B. Alexander, S. B. Waters, K. P. Plucknett, K. Hirao, and M. E. Brito, ''Microstructural Design of Silicon Nitride with Improved Fracture Toughness: II, Effect of Additives,'' *J. Am. Ceram. Soc.*, **81** [11] 2831–40 (1998).

[26]T. Kawashima, H. Okamoto, H. Yamamoto, and A. Kitamura, ''Characteristic Variety of Silicon Nitride Made Through Microstructural Control''; pp. 135–46 in *Silicon Nitride Ceramics 2*. Edited by M. Mitomo and S. Somiya. Uchida Rokakuho Publishing Co., Ltd., Tokyo, Japan, 1990.

[27]D. A. Bonnell, M. Rühle, and T. Y. Tien, ''Redistribution of Aluminum Ions During Processing of SiAlON Ceramics,'' *J. Am. Ceram. Soc.*, **69** [8] 623–27 (1986).

[28]K. B. Alexander, P. F. Becher, P. M. Rice, D. Braski, and E. Y. Sun, ''Microstructure and Microchemistry of Interfaces in Structural Ceramic Composites''; pp. 167–78 in Materials Research Society Symposium Proceedings, Vol. 458, *Interfacial Engineering for Optimized Properties.* Materials Research Society, Pittsburgh, PA, 1997.

[29]E. Y. Sun, C. H. Hsueh, and P. F. Becher, ''*R*-Curve Response of SiC Whisker-Reinforced Alumina: Microstructural Influence''; pp. 223–28 in Materials Research Society Symposium Proceedings, Vol. 409, *Fracture-Instability Dynamics, Scaling and Ductile/Brittle Behavior.* Edited by R. B. Selinger, J. J. Mecholsky, A. E. Carlsson, and E. R. Fuller. Materials Research Society, Boston, MA, 1996.

[30]E. S. Kang; unpublished results.

[31]P. F. Becher, E. Y. Sun, C. H. Hsueh, K. B. Alexander, S. L. Hwang, S. B. Waters, and C. G. Westmoreland, ''Debonding of Interfaces Between β-Silicon Nitride Whiskers and Si-Al-Y Oxynitride Glasses,'' *Acta Metall.*, **44** [10] 3881–93 (1996).

[32]C. W. Li, S.-C. Lui, and J. Gldacker, ''Relation Between Strength, Microstructure, and Grain-Bridging Characteristics in *In Situ* Reinforced Silicon Nitride,'' *J. Am. Ceram. Soc.*, **78** [2] 449–59 (1995).

[33](a) C. H. Hsueh, ''Effects of Aspect Ratios of Ellipsoidal Inclusions on Elastic Stress Transfer of Ceramic Composites,'' *J. Am. Ceram. Soc.*, **72** [2] 344–47 (1989). (b) C. H. Hsueh, R. J. Young, X. Yang, and P. F. Becher, ''Stress Transfer in a Model Composite Containing a Single Embedded Fiber,'' *Acta Metall. Mater.*, **45** [4] 1469–76 (1997). □